FULL PAPER

m-Indolocarbazole Derivative as a Universal Host Material for RGB and White Phosphorescent OLEDs

*Cheng-Chang Lai, Min-Jie Huang, Ho-Hsiu Chou, Chuang-Yi Liao, Pachaiyappan Rajamalli, and Chien-Hong Cheng**

The host materials designed for highly efficient white phosphorescent organic light-emitting diodes (PhOLEDs) with power efficiency (PE) >50 lm W^{-1} and low efficiency roll-off are very rare. In this work, three new indolocarbazole-based materials (ICDP, 4ICPPy, and 4ICDPy) are presented composed of 6,7-dimethylindolo[3,2-*a*]carbazole and phenyl or 4-pyridyl group for hosting blue, green, and red phosphors. Among this three host materials, 4ICDPy-based devices reveal the best electroluminescent performance with maximum external quantum efficiencies (EQEs) of 22.1%, 27.0%, and 25.3% for blue (FIrpic), green (*fac*-Ir(ppy)$_3$), and red ((piq)$_2$Ir(acac)) PhOLEDs. A two-color and single-emitting-layer white organic light-emitting diode hosted by 4ICDPy with FIrpic and Ir(pq)$_3$ as dopants achieves high EQE of 20.3% and PE of 50.9 lm W^{-1} with good color stability; this performance is among the best for a single-emitting-layer white PhOLEDs. All 4ICDPy-based devices show low efficiency roll-off probably due to the excellent balanced carrier transport arisen from the bipolar character of 4ICDPy.

1. Introduction

Over the past few decades, white organic light-emitting diodes (WOLEDs) have been of great interest with respect to their promising application in lighting and display.[1] Fully phosphorescent WOLEDs are particularly attractive to be a potential approach in realizing bright lighting sources with high performance, because phosphorescent emitting materials are capable of harvesting both the singlet and the triplet excitons, resulting in internal quantum efficiencies of 100%.[2] To achieve excellent performance of a phosphorescence-based device, the phosphor has to be incorporated into an appropriate host to avoid concentration quenching by triplet–triplet annihilation (TTA). Therefore, the design of efficient host is important for developing high-performance phosphorescent organic light-emitting diodes (PhOLEDs).[3] In general, an efficient host must fulfill the following criteria. First, the triplet energy gap of the host should be suitably higher than that of the emitting phosphor to ensure exothermic energy transfer from the host to the dopant and to confine the triplet excitons on the dopant molecules.[1e,4] Second, the host material should possess high carrier drift mobilities and balanced electric fluxes to increase the electron and hole recombination within the emitting layer. Finally, a high glass transition temperature (T_g) is necessary for a host material to increase the thermal and morphological stability of the device and thus lengthen the device lifetime.[5] Based on the above-mentioned requirements for hosts, many efficient host materials have been developed for PhOLEDs. Among these high-performed hosts, the bipolar materials were found to be the most promising candidates to date.[6] Through the incorporation of electron-donating and electron-accepting moieties in a molecule, the resulting host material exhibits excellent electron and hole transporting behaviors, leading to good balance of the charge carrier fluxes. Compared with traditional *p*-type or *n*-type host materials, a bipolar host provides more balanced carrier injection and transport, which leads to a broader recombination zone within the emissive layer, reduces the occurrence of TTA, and hence gives highly efficient PhOLEDs with lower efficiency roll-off.[7]

In recent year, several research groups had attempted to synthesize and use bipolar materials as universal hosts for high-performance RGB PhOLEDs and WOLEDs.[8] The use of a sole bipolar host for a WOLED not only greatly simplifies the fabrication processes, but also effectively reduces the unwanted power loss arisen from multiple emitting layers. Nevertheless, a great disadvantage of a bipolar host is the reduced triplet energy gap due to the intramolecular charge transfer from the donor to acceptor moieties.[9] This limits the application of universal bipolar hosts in blue PhOLEDs and WOLEDs.[6] Hence, only few examples of highly efficient universal hosts are reported in the literature. In 2010, our group presented the first universal bipolar host bis-[4-(*N*-carbazolyl)phenyl]phenylphosphine oxide (BCPO) comprising a phosphine oxide as the electron acceptor and two carbazole groups as the electron donor groups. The material was employed in blue, green, and red phosphorescent devices to afford extremely high device efficiencies.[5] The first example of the white light-emitting devices

C.-C. Lai, Dr. M.-J. Huang, Dr. H.-H. Chou, Dr. C.-Y. Liao
Dr. P. Rajamalli, Prof. C.-H. Cheng
Department of Chemistry
National Tsing Hua University
Hsinchu 30013, Taiwan
E-mail: chcheng@mx.nthu.edu.tw

DOI: 10.1002/adfm.201502079

using universal bipolar host materials was demonstrated by Ma and co-workers.[10] The white device hosted by *p*-BISiTPA, a bipolar material integrated with silicon-bridged triphenylamine and benzimidazole segments, gave maximum efficiencies of 19.1% and 51.9 lm W^{-1}, and showed low efficiency roll-off at high luminance. Recently, a new fluorene-based bipolar host CzFCN was developed consisting of electron-rich carbazole and electron-deficient nitrile groups.[11] The CzFCN-based devices yielded EQEs of 20.7% for red, 20.0% for green, 16.5% for blue, and 15.7% for white PhOLEDs with the same device structure. Although several universal bipolar hosts have been applied in WOLEDs, to develop a sole host suitable for different color dopants still is a critical issue for the realization of cost-effective white device with high power efficiency and low efficiency roll-off at high luminance.

The compounds with an indolocarbazole core have been extensively applied in optoelectronics owing to the advantages such as large planar rigid conjugated structures, excellent hole transporting ability, and outstanding morphological stability and thermal durability.[12] In OLEDs, some indolocarbazole derivatives have been used as the host materials for green, orange, and red phosphorescent devices as well as hole-transporting materials and deep-blue emitters.[13] However, the low triplet energy of indolocarbazole-containing materials limits the use of them as the core of bipolar host materials for blue PhOLEDs. To further develop indolocarbazole-based hosts for blue phosphorescent devices, in this study, we design three new host materials, ICDP, 4ICPPy, and 4ICDPy for RGB phosphorescence devices via the integration of 6,7-dimethylindolo[3,2-*a*]carbazole and phenyl or 4-pyridyl moieties. Indolo[3,2-*a*]carbazole core is chosen because it is anticipated to have a higher triplet energy than other indolocarbazole isomers due to its bridged *meta* structure.[14] The pyridine unit is introduced to enhance the electron transport properties and increase the thermal stability of the material.[4e,15] Among these three hosts, 4ICDPy exhibited the best device performance with EQEs of 22.1%, 27.0%, and 25.3% for blue, green, and red PhOLEDs, respectively. A fully phosphorescent 4ICDPy-based WOLED with very high efficiencies without out coupling was also realized. Interestingly, this WOLED showed remarkable color stability with a low efficiency roll-off at high brightness. To the best of our knowledge, this is the first work to develop an indolocarbazole-based universal host that renders high quantum efficiency in the RGB and white phosphorescent OLEDs.

2. Results and Discussion

2.1. Synthesis and Characterization of Indolocarbazole-Based Hosts

Scheme 1 outlines the synthetic routes for indolo[3,2-*a*]carbazole-based host materials. ICDP and 4ICDPy were synthesized by *N*-arylation of 6,7-dimethylindolo[3,2-*a*]carbazole (DMIC) with iodobenzene and 4-bromopyridine, respectively, in the presence of $Pd_2(dba)_3$, tri-*t*-butylphosphine, and sodium *t*-butoxide.[16] The preparation of 4ICPPy was carried out via a two-step cross-coupling reactions. The details for the synthesis of ICDP, 4ICPPy, and 4ICDPy are described in the Experimental Section. All products were characterized by their NMR spectroscopy and high-resolution mass, and the molecular structure of ICDP, 4ICPPy, and 4ICDPy were further verified by single-crystal X-ray diffraction analysis.

Figure 1 depicts the crystal structures and molecular packing diagrams of these three host materials. In all these crystals, the central indolocarbazole groups are nearly planar with small torsion angles of ≈5°. The two aromatic rings attached to the nitrogen atoms of each indolocarbazole group are twisted out of the indolocarbazole plane with dihedral angles of 72.7° and 49.4° for ICDP, 53.3° and 50.5° for 4ICPPy, and 45.0° and 38.3° for 4ICDPy. Further, for the two dihedral angles in each compound, the one near to the methyl group is larger than the other because of the repulsion of the aromatic ring with the methyl group. These noncoplanar conformations effectively reduce the degree of π-conjugation between indolocarbazole and the aryl rings and thus maintain the high triplet energy for these host materials. For the crystal packings, both ICDP and 4ICPPy molecules show intermolecular π,π-aggregation of the indolocarbazole backbones in a slipped face-to-face fashion with an interplanar distance of 3.37 and 3.49 Å, respectively.

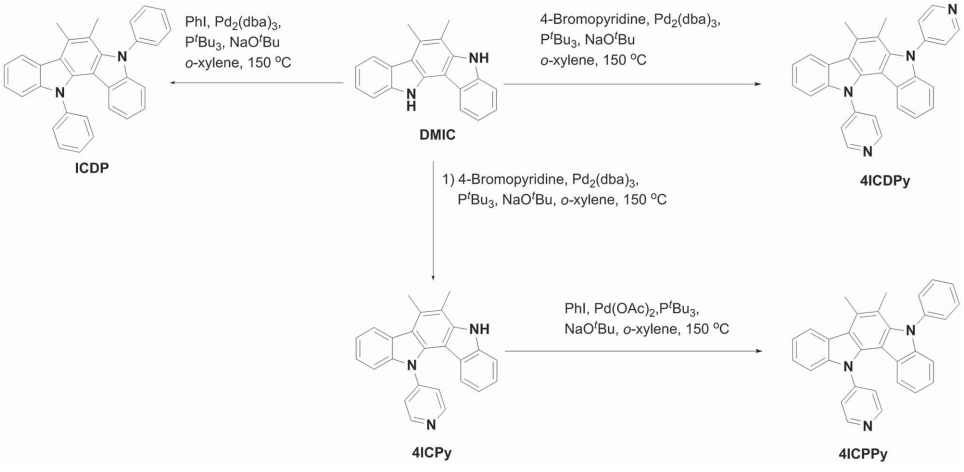

Scheme 1. Synthsis of indolo[3,2-*a*]carbazole derivatives ICDP, 4ICDPy, and 4ICPPy.

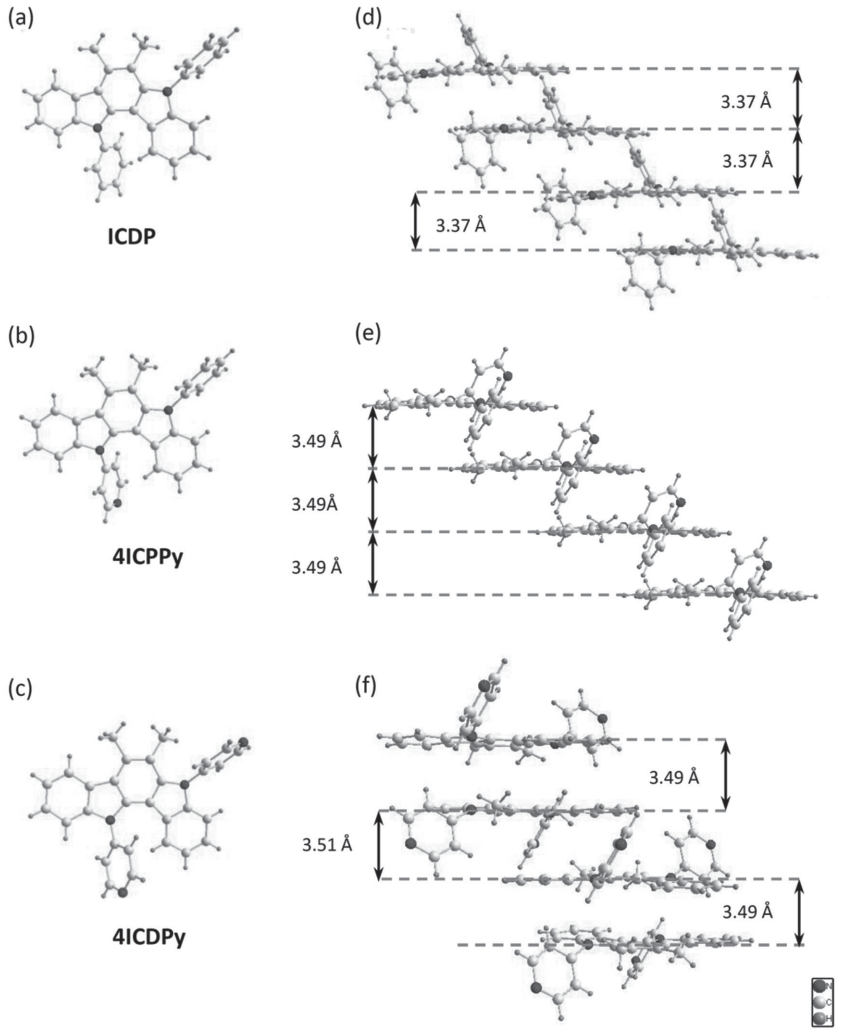

Figure 1. ORTEP diagrams and molecular packing patterns of a) ICDP, b) 4ICPPy, and c) 4ICDPy. Thermal ellipsoids are drawn at 50% probability.

Different from the packing of ICDP and 4ICPPy, 4ICDPy forms a dimer-brickwall motif, in which two neighboring indolocarbazole moieties are packed via head-to-tail dimerization with stacking distance of 3.49 Å. Such π-stacking arrangement via indolocarbazole cores would be beneficial to produce high carrier-transport ability and thus enhance electroluminescence performance.

2.2. Optical Properties and Theoretical Calculations

The UV–vis absorption and photoluminescent (PL) spectra of these indolocarbazole-based materials in methylene chloride and neat film were measured and are displayed in **Figure 2** and summarized in **Table 1**. For better comparison, the absorption and emission spectra of the parent molecule indolo[3,2-*a*]carbazole (DMIC) are also incorporated. As displayed in Figure 2, the absorption patterns of all these materials are similar, indicating that these absorptions are mainly contributed by the electronic transitions associated with the indolocarbazole moiety. The strong absorption peak at 310 nm can be ascribed to the indolocarbazole-centered π–π^* transition, and the weaker absorptions around 345 and 360 nm are assigned to the n–π^* transition of indolocarbazole. However, it is worth noting that the PL spectra in DCM for 4ICPPy and 4ICDPy are distinctly different from that of ICDP and DMIC, in which both 4ICPPy and 4ICDPy show a pronounced dual emission, while ICDP and DMIC exhibit an emission with vibronic feature. To look into their optical properties, the emission spectra of these materials were studied in various solutions (see Figure S1 in the Supporting Information). The fine-structured FL profiles of ICDP do not change significantly with the solvent used, suggesting that its emission arises from a locally excited (LE) state of the molecule. In the PL spectra of 4ICPPy and 4ICDPy, a solvent-independent emission in near-ultraviolet region and a solvent-dependent broad peak at longer wavelength region are observed. This finding indicates that their emitting state originates from a combination of LE and ICT (intramolecular charge transfer) character. Similar phenomenon and interpretation were also found in the other efficient host materials reported previously.[17]

As displayed in Figure S1, Supporting Information, the fluorescence intensity efficiency of 4ICPPy and 4ICDPy are found to quickly decrease with the increase in solvent polarity compared to that of ICDP. The decrease of emission intensity in polar solvent can be ascribed to the formation of ICT state because the dipole–dipole interaction between the ICT state of molecule and polar solvent facilitates nonradiative relaxation rather than fluorescence emission, leading to lower PL efficiency in polar environment. The influence of solvent polarity on the emission features of 4ICPPy and 4ICDPy can be further assessed via Lippert–Mataga equation[18] (see Tables S1 and S2, Supporting Information, and Lippert–Mataga analysis in the Supporting Information for details). By plotting the Stock shift (ν_a–ν_f) against the solvent polarity (f), the difference between the excited-state and ground-state dipole moments ($\Delta\mu = \mu_e - \mu_g$) was derived from the slopes of the linear fitting (Figure S2, Supporting Information). Ground-state dipole moments (μ_g), determined from density functional theory (DFT) calculation with B3LYP/6–31g* basis set, are 3.7 D for 4ICPPy and 1.4 D for 4ICDPy. Accordingly, excited-state dipole moments (μ_e) for the LE and CT states of 4ICPPy are calculated to be 8.9 and 13.9 D, respectively, while 4ICDPy has a μ_e of 5.5 D for the LE state and 10.6 D for the CT state. It is worth noting that the μ_e values of CT states for 4ICPPy and 4ICDPy are much smaller than usual CT emitters,[19] indicative of a relative weak ICT progress for emissive state of 4ICPPy and 4ICDPy due to weak

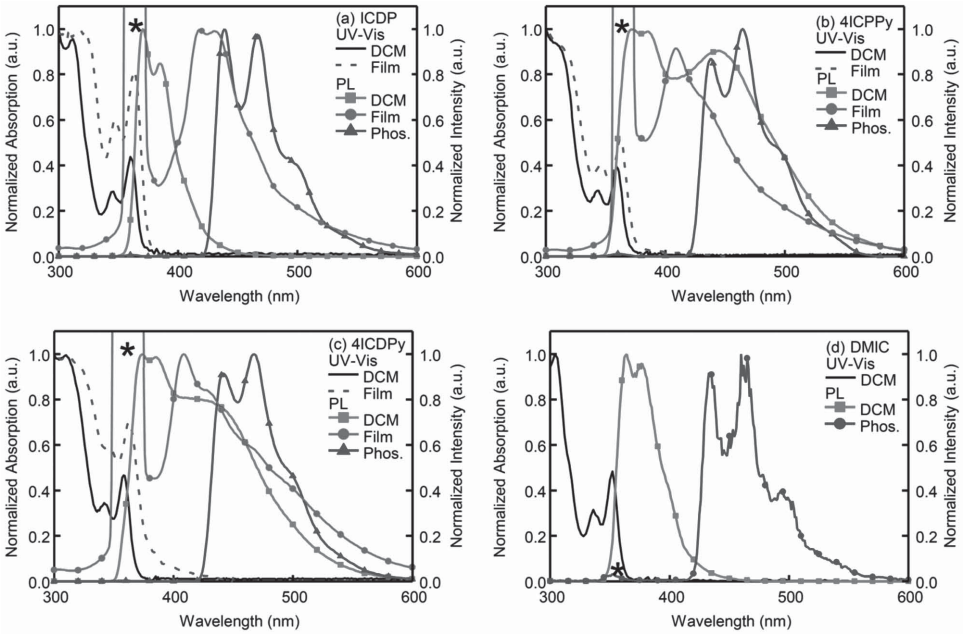

Figure 2. UV–vis absorption, fluorescence, and phosphorescence spectra of a) ICDP, b) 4ICPPy, c) 4ICDPy, and d) the parent molecule DMIC. Absorption and fluorescence were measured in dichloromethane and thin film at RT. Phosphorescence spectra were obtained at 77 K in 2-methyltetrahydrofurane. The excitation peak is marked with an asterisk.

electron withdrawing ability of 4-pyridyl group. Thus, the CT emissions of 4ICPPy and 4ICDPy show a slightly redshift as the solvent polarity increases.

To get more insights into the nature of emission for these molecules, natural transition orbitals (NTOs) of the lowest excited state were simulated and evaluated by using the method of time-dependent DFT (TD-DFT) at B3LYP/6–31G* level (Table S3, Supporting Information). In the S_1 state of ICDP, both the hole and particle NTOs are delocalized over the molecular backbone composed of indolocarbazole core and the phenyl groups, indicative of a predominant LE state for the low-lying singlet excited state. In contrast, the S_1 of 4ICPPy and 4ICDPy exhibit an ICT from the indolocarbazole units to the 4-pyridyl groups as well as the indolocarbazole-based LE transition, leading to a dual-emission feature in their PL spectra. The simulated results of the excited-state property agree well with the observed spectral behavior in solvatochromic experiments. In addition, the emission bands of host materials in the neat film are substantially red-shifted by 34–46 nm relative to those in solution. The large red shift in the film is likely the result of strong π–π stacking between the adjacent indolocarbazole moieties, and the solid state polarization effect resulting from the polarity of the materials. All phosphorescent spectra were measured in the 2-methyltetrahydrofurane matrix at 77 K. The phosphorescent emission spectra of these hosts reveal similar well-defined patterns to that of the parent molecule DMIC. The triplet energy levels were estimated to be 2.83, 2.83, and 2.81 eV, respectively for ICDP, 4ICPPy, and 4ICDPy, calculated from the highest-energy vibronic sub-band of the phosphorescence spectra. These values are very close to the triplet energy level of DMIC (2.83 eV). Thus, the introduction of a phenyl or 4-pyridyl group at the *N*-positions of DMIC does not significantly influence the triplet energy of the whole molecules, consistent with the highly twisted structure between the indolocarbazole moiety and aryl group which reduces the interaction between the two moieties and keeps the triplet energy of ICDP, 4ICPPy, and 4ICDPy very close to that of DMIC. The high triplet energies of these indolocarbazole-based materials are essential to serve as host materials for blue PhOLED and white PhOLED.

Table 1. Summary of physical properties for ICDP, 4ICPPy, and 4ICDPy.

Materials	λ_{abs} [nm]		λ_{fl} [nm]		λ_{Phos} [nm]	E_g/E_T[a)] [eV]	HOMO[b)]/LUMO [eV]	$T_g/T_c/T_m/T_d$ [°C]
	Sol.[c)]	Film	Sol.[c)]	Film	Sol.[d)]			
ICDP	313, 345, 361	323, 346, 363	371, 385	417, 430	439, 467, 495	3.31/2.83	5.29/1.98	63/185/225/328
4ICPPy	310, 343, 359	345, 363	372, 385, 445	409, 430	438, 465, 490	3.30/2.83	5.38/2.08	104/N.D.[e)]/242/308
4ICDPy	310, 344, 359	346, 364	374, 381, 431	408, 430, 462	441, 467, 492	3.30/2.81	5.47/2.17	114/183/296/345

[a)]The band gap (E_g) energies were estimated from absorption edges. E_T was determined from the high-energy emission maxima in the phosphorescence spectra; [b)]Redox measurements were carried out in dichloromethane containing 1×10^{-1} M host material using Cp_2Fe/Cp_2Fe^+ as reference;[c)] Measured in dichloromethane solution with the concentration of 10^{-5} M; [d)]Measured in 2-methyltetrahydrofurane at 77 K; [e)]N.D. = not detected.

2.3. Thermal Analysis and Electrochemistry

The thermal stability of ICDP, 4ICPPy, and 4ICDPy were determined by thermogravimetric analysis (TGA) and differential scanning calorimetry (DSC). The resulting melting point (T_m), glass-transition temperature (T_g), crystallization temperature (T_c), and decomposition temperature (T_d, corresponding to 5% weight loss) are shown in Figures S3 and S4, Supporting Information, and summarized in Table 1. All compounds are thermally stable with T_d values in the range of 308–345 °C, and the T_m of these materials are in the range of 225–296 °C. Both ICDP and 4ICDPy exhibit distinct T_c at about 183 °C, but no T_c was found for 4ICPPy. Similar twisted configurations of ICDP and 4ICDPy lead to very close T_c values. Notably, the T_g values of 4ICPPy and 4ICDPy are 40–50 °C higher than that found for ICDP, suggesting that the presence of 4-pyridyl group improves the thermal stability. Such increase in T_g value could be ascribed to a strong dipole–dipole interaction in the solid state arisen from the polarity of 4ICPPy and 4ICDPy. To further analyze their morphology stability, atomic force microscopy (AFM) was employed to acquire the topography of these hosts after annealing at 60 °C for 18 h (Figure S5, Supporting Information). The organic films exhibit a root-mean-square roughness (R_{rms}) of 1.32, 0.39, and 0.33 nm for ICDP, 4ICPPy, and 4ICDPy, respectively. The thin films of 4ICPPy and 4ICDPy are significantly smoother than that found for ICDP. The AFM results show that 4ICPPy and 4ICDPy give better thermal and morphological stability in the neat film.

The redox properties of all materials were examined by cyclic voltammetry (CV), as shown in Figure S6, Supporting Information. In the anodic scan, the quasi-reversible oxidation waves take place at 0.89, 0.98, and 1.07 V relative to the ferrocence/ferrocenium (Fc/Fc^+) couple for ICDP, 4ICPPy, and 4ICDPy, respectively. No reduction wave was observed in the cathodic sweep for all materials. The results of CV studies reveal that the oxidation potentials of indolocarbazole-based materials shift to the more positive region as the number of pyridine substituent increases. This observation suggests that the oxidation occurs in the indolocarbazole backbone and the oxidation becomes difficult in the presence of electron-withdrawing 4-pyridyl group. The HOMO energy levels were calculated using the equation HOMO = E_{ox} + 4.8 eV, while the LUMO values were estimated by deducting the optical band gap from HOMO energy. The reported HOMO/LUMO values of ICDP, 4ICPPy, and 4ICDPy are 5.29/1.98, 5.38/2.08, and 5.47/2.17 eV, respectively.

2.4. Charge-Carrier Mobility

To evaluate the carrier transport properties of these materials, the hole-only and electron-only devices were fabricated with the structures of ITO (indium tin oxide)/MoO_3 (1 nm)/host (100 nm)/MoO_3 (10 nm)/Al (100 nm) and ITO/Ca (5 nm)/host (100 nm)/LiF (1 nm)/Al (100 nm), respectively. By employing space-charge limited currents (SCLC) method, the field-dependent carrier mobility (μ) was derived from the J–V curves (Figure S7, Supporting Information) of hole-only and electron-only devices based on the Mott–Gurney equation,[20] which is expressed as follows

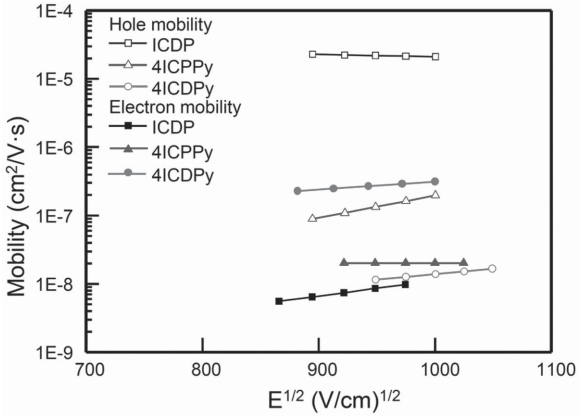

Figure 3. Semilogarithmic plots of hole and electron mobility versus $E^{1/2}$ for ICDP, 4ICDPy, and 4ICPPy.

$$J = \frac{9}{8}\varepsilon\varepsilon_0\mu\frac{E^2}{L} \quad (1)$$

where E is the electric field, ε_0 is the free-space permittivity ($\varepsilon_0 = 8.85 \times 10^{-14}$ C V^{-1} cm), ε is the relative dielectric constant (assumed to be 3.0), and L is the thickness of the host material. As displayed in **Figure 3**, the obtained mobility follows the universal Poole–Frenkel relationship which predicts an exponential increase in hole and electron mobility as a function of the square root of the electric field.[21] The electron mobility of these three materials increases in the order ICDP < 4ICPPy < < 4ICDPy, but the reverse trend was observed for the hole mobility of these materials. For ICDP and 4ICPPy, the hole mobility is over one order of magnitude higher than the electron mobility because of the π–π interaction between indolocarbazole moieties in the film and the electron-donating nature of the moiety, which make hole hopping easier among the adjacent molecules. The introduction of the pyridine moiety to the molecule significantly increases electron mobility and reduces the hole mobility, leading to carrier mobility balance.[4e,22] Based on the above mobility studies, we can conclude that, among the three hosts, 4ICPPy and 4ICDPy have the bipolar feature in view of their relatively balanced electron and hole mobility. On the other hand, ICDP has good hole transporting ability, but probably not a good bipolar material.

2.5. Electroluminescence Devices

To demonstrate the potential of indolo[3,2-*a*]carbazole-based materials as the hosts for phosphorescence organic light-emitting devices, we first fabricated blue devices B1–B3 by utilizing iridium(III) bis(4,6-difluorophenylpyridinato-*N*,$C^{2'}$)picolinate (FIrpic) as the dopant and the indolocarbazole-based materials as the hosts. The device configuration consists of ITO/TAPC (50 nm)/ICDP (10 nm)/host: 8% FIrpic (30 nm)/3TPYMB (5 nm)/BCP (40 nm)/LiF (1 nm)/Al (100 nm), where the host is ICDP, 4ICPPy, or 4ICDPy for B1-B3, respectively. In the device, TAPC (1-bis[4-[*N*,*N*-di(4-tolyl)amino]phenyl]cyclohexane) acts as the hole-transporting material and BCP (bathocuproine) is the electron-transporting material. In addition, ICDP and

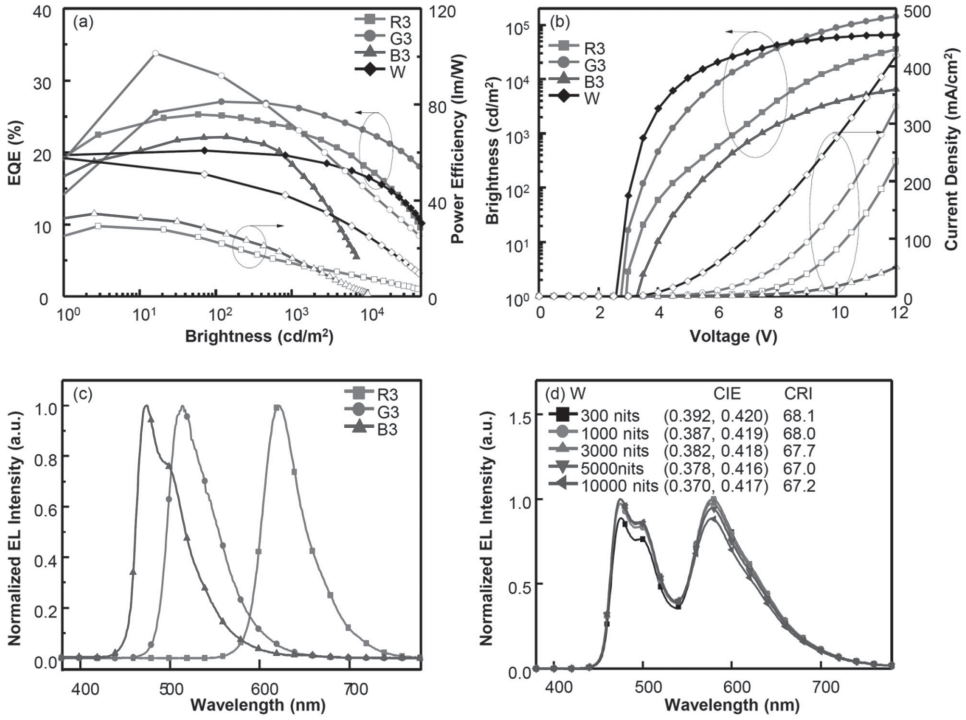

Figure 4. Performance of the 4ICDPy-based devices. a) Plots of EQE (solid) and power efficiency (hollow) as a function of brightness. b) Current density–voltage–luminance (*J*–*V*–*L*) characteristics. c) EL spectra of devices B3, G3, and R3. d) EL spectra of white device W at different brightness.

3TPYMB (tri[3-(3-pyridyl)mesityl]borane) serve as the exciton-blocking layer to prevent dopant or host triplet excitons in the emissive layer to diffuse to TAPC and BCP layers. The electroluminescent characteristic plots of these devices are displayed in **Figure 4**, Figures S9 and S10, Supporting Information, and the key data are summarized in **Table 2**. All EL spectra of devices B1–3 show the typical emission of the phosphor FIrpic with main peak at 475 nm and a shoulder peak at 500 nm, suggesting full energy transfer from these hosts to iridium dopant. Among these three devices, B3 using 4ICDPy as the host reveals a maximum current efficiency (CE) as high as 45.5 cd A^{-1}, a maximum power efficiency (PE) of 34.5 lm W^{-1}, and a maximum external quantum efficiency (EQE) of 22.1%, significantly higher than those found in devices B1 and B2 hosted by ICDP (CE = 25.0 cd A^{-1}, PE = 14.0 lm W^{-1}, and EQE = 10.5%) and 4ICPPy (CE = 34.4 cd A^{-1}, PE = 24 lm W^{-1}, and EQE = 13.4%), respectively. The best performance of device B3 can be attributed to the more improved electron injection and the carrier balance resulted from the high electron mobility of 4ICDPy. It is worth noting that device B2 hosted by 4ICPPy

Table 2. Performance characteristics of indolocarbazole-based OLEDs.

Device	Host	V_{on}[a)] [V]	L_{max} [cd m^{-2}, V]	EQE_{max} [%, V]	CE_{max} [cd A^{-1}, V]	PE_{max} [lm W^{-1}, V]	EQE[b)] [%, V]	CIE[c)] (*x*, *y*)
B1[d)]	ICDP	3.0	22201, 14.0	10.5, 6.5	25.0, 6.5	14.0, 5.5	10.4, 7.4	(0.15, 0.37)
B2[d)]	4ICPPy	3.0	14380, 15.5	13.4, 5.5	34.4, 5.5	24.0, 4.0	11.7, 7.1	(0.13, 0.31)
B3[d)]	4ICDPy	3.2	10030, 16.0	22.1, 5.0	45.4, 5.5	34.5, 4.0	18.4, 7.5	(0.14, 0.32)
G1[e)]	ICDP	2.5	30935, 10.5	10.0, 3.0	34.1, 3.0	35.7, 3.0	8.3, 3.6	(0.24, 0.61)
G2[e)]	4ICPPy	2.5	91242, 15.0	23.9, 3.0	86.9, 3.0	90.8, 3.0	23.2, 3.3	(0.24, 0.64)
G3[e)]	4ICDPy	2.5	158708, 13.5	27.0, 3.5	102.4, 3.5	101.3, 3.5	26.4, 4.3	(0.24, 0.64)
R1[f)]	ICDP	2.8	14408, 13.0	4.9, 5.0	6.7, 5.0	5.5, 3.5	5.3, 5.3	(0.59, 0.33)
R2[f)]	4ICPPy	2.5	46358, 15.5	23.9, 3.5	31.1, 3.5	31.4, 3.0	22.0, 5.5	(0.66, 0.33)
R3[f)]	4ICDPy	2.7	56841, 15.0	25.3, 4.0	31.5, 4.0	30.0, 3.0	23.4, 6.6	(0.67, 0.33)
W[g)]	4ICDPy	2.5	65468, 12.0	20.3, 3.0	48.7, 3.0	50.9, 3.0	19.4, 3.6	(0.37, 0.42)

[a)]The applied voltage required for 1 cd m^{-2}; [b)]@ 1000 nits; [c)]EL was measured at 8 V; [d)]ITO/TAPC (50 nm)/ICDP (10 nm)/host: 8% FIrpic (30 nm)/3TPYMB (5 nm)/BCP (40 nm)/LiF (1 nm)/Al (100 nm); [e)]ITO/NPB (10 nm)/TAPC (20 nm)/host: 6% $Ir(ppy)_3$ (25 nm)/TPBI (60 nm)/LiF (1 nm)/Al (100 nm); [f)]ITO/NPB (15 nm)/TCTA (10 nm)/host: 4% $(piq)_2Ir(acac)$ (25 nm)/BCP (10 nm)/ Alq_3 (50 nm)/LiF (1 nm)/Al (100 nm); [g)]ITO/NPB (10 nm)/TAPC (20 nm)/4ICDPy: 10% FIrpic: 0.2% $Ir(pq)_3$ (30 nm)/TPBI(50 nm)/LiF (1 nm)/Al (100 nm).

with a bipolar property does not achieve good efficiency for blue PhOLED. This result can be explained by the more serious carrier trapping of the 4ICPPy-based device[23] than that of 4ICDPy because of the larger difference in HOMO levels between FIrpic and 4ICPPy (Figure S8, Supporting Information).

Next, we examine the performance of these three materials as the hosts for low energy triplet emitters. The green and red devices were fabricated using the structures: ITO/NPB (10 nm)/TAPC (20 nm)/host: 6% $Ir(ppy)_3$ (25 nm)/TPBI (60 nm)/LiF (1 nm)/Al (100 nm) and ITO/NPB (15 nm)/TCTA (10 nm)/host: 4% $(piq)_2Ir(acac)$ (25 nm)/BCP (10 nm)/Alq_3, 50 nm)/LiF (1 nm)/Al (100 nm), where NPB = 4,4′-bis[*N*-(1-naphthyl)-N-phenylamino]biphenyl, TPBI = 1,3,5-tris[*N*-(phenyl)benzimidazole]benzene and Alq_3 = tris(8-hydroxyquinolinato)aluminum. The three green devices G1–3 using $Ir(ppy)_3$ as the dopant all exhibit green emissions peaked at ≈512 nm from $Ir(ppy)_3$ in their EL spectra. Of the three red devices fabricated, R2 and R3 exhibit pure red emission of $(piq)_2Ir(acac)$, but R1 gave, in addition to the red emission of $(piq)_2Ir(acac)$, an unexpected blue emissions plausibly from BCP and Alq_3 in the EL spectrum. The additional blue emissions are likely due to the high hole mobility of ICDP, leading to exciton recombination within BCP and Alq_3 layers. Devices G3 and R3, both hosted by 4ICDPy, achieve a low turn-on voltage of ≈2.5 V and give excellent performance for green and red PhOLED with maximum efficiencies of 27.0%, 102.4 cd A^{-1}, 101.3 lm W^{-1} and 25.3%, 31.5 cd A^{-1}, 30.0 lm W^{-1}, respectively. In addition, both devices exhibit very low efficiency roll-off. For instance, device G3 affords a CE of 99.8 cd A^{-1} and EQE of 26.4% with an EQE roll-off of 2.2% at the luminance of 1000 cd m^{-2}. The roll-off for device R3 at the luminance of 1000 cd m^{-2} is 7.5%. Such small efficiency roll-off is ascribed to the balanced charges and wide recombination zone in the EMLs arising from the bipolar behavior of 4ICDPy. Surprisingly, the red and blue devices hosted by ICDP give lower efficiency roll-off at high luminance than those of 4ICDPy (Figure S10, Supporting Information). This result is probably because the good hole mobility of ICDP leads to little charge accumulation at the interface between the emitting layer and hole-blocking layer, which reduces exciton–polaron quenching and thus result in extremely low efficiency roll-off for ICDP-based red and blue devices.[24] Among the three indolocarbazole-based hosts, 4ICDPy gives the best EQEs of 22.1%, 27.0%, and 25.3% for blue, green, and red PhOLEDs, respectively. These results are comparable to the best performance of RGB devices using a universal host.[8c,25]

Finally, the excellent performance of 4ICDPy-based RGB devices prompts us to examine the use of 4ICDPy as the host for single-host WOLED. A two-element WOLED was fabricated under the device configuration: ITO/NPB (10 nm)/TAPC (20 nm)/4ICDPy: 10% FIrpic: 0.2% $Ir(pq)_3$ (30 nm)/TPBI (50 nm)/LiF (1 nm)/Al (100 nm). Single-layer EML was chosen because bipolar 4ICDPy can efficiently broaden the exciton-formation zone and reduce exicton drift, resulting in the enhancement of device efficiency and color stability.[26] The device performance of WOLED (device W) is also summarized in Table 2, and the corresponding EQE-luminance-PE curve as well as its EL spectrum are displayed in Figure 4. Device W shows a balanced blue and orange emission in the EL spectrum, and no significant color variation is observed over a wide range of brightness. The CIE coordinates vary slightly from (0.39, 0.42) to (0.37, 0.42) as the brightness increases from 300 to 10 000 cd m^{-2}, demonstrating a highly stable chromaticity for device W. Because of a two-color system, a relatively low CRI (color rendering index) value of 68 is obtained for this 4ICDPy-based white device. Similar to the behavior of RGB devices, the white device hosted by 4ICDPy shows relatively low turn-on voltage of 2.5 V and offers an EQE of 20.3% and CE of 48.7 cd A^{-1}. At a high brightness of 1000 cd m^{-2}, the EQE remains at 19.4% with a low roll-off value of 4.4%.[27] In particular, the PE of device W is as high as 50.9 lm W^{-1}, which is among the best of two-color white PhOLEDs using a universal host.[17c,25a,28] Thus, 4ICDPy is demonstrated as universal hosts for WOLED.

3. Conclusions

In summary, we have synthesized three indolocarbazole-based materials, ICDP, 4ICPPy, and 4ICDPy for use as universal hosts for blue, green and red PhOLEDs and white OLEDs. Photophysical and DFT analysis reveal that the excited state of 4ICDPy and 4ICPPy contains a combined character of local and charge-transfer state, leading to dual emissions in their PL spectra, which are not seen for ICDP. The introduction of 4-pyridyl group(s) onto the indolocarbazole core structure renders good thermal stability, homogeneous morphology, and balanced carrier transporting ability without significantly lowering their triplet energy levels. More importantly, highly efficient blue, green, red PhOLEDs with EQEs of 22.1, 27.0, and 25.3%, respectively, can be realized by using 4ICDPy as the host. The two-color, single-host white device using 4ICDPy as the host exhibits superior EL performance and color stability with EQE of 20.3% and PE of 50.9 lm W^{-1}. The results appears to be the best among the reported single-host WOELDs. Moreover, all the devices hosted by 4ICDPy reveal low turn-on voltage and low efficiency roll-off at high luminance. These findings demonstrate that the introduction of 4-pyridyl groups into indolocarbazole is an effective approach to design universal host materials for highly efficient RGB PhOLEDs and WOLEDs.

4. Experimental Section

General Information: All chemicals were purchased from Alfa Aesar and Strem. The solvents were dried according to the standard procedures. Other reagents were used as supplied unless otherwise stated. 6,7-Dimethylindolo[3,2-*a*]carbazole (DMIC) was prepared by following the method described in the literature.[16] All materials used for electroluminescence devices were further purified by temperature gradient vacuum sublimation. ^1H and ^{13}C NMR spectra were measured with a Varian Mercury 400 spectrometer and referenced to residual peak of $CDCl_3$ solvent as internal standard. Mass spectra were obtained on a Jeol JMS-SX102A HRGC/LC/MS instrument. Steady-state spectra of absorption and emission were recorded on a Hitachi U-3310 spectrophotometer and Hitachi F-4500 fluorimeter, respectively. Thermal gravimetric analysis (TGA) was performed on TGA 2050 (TA Instruments) under a nitrogen atmosphere to acquire the decomposed temperature corresponding to 5% weight loss. The measurements of the glass transition temperature were carried out under a nitrogen atmosphere by DSC Q10 instrument from TA Instruments. The morphologies of the host films were obtained under ambient temperature by using tapping-mode

atomic force microscopy (TM-AFM) from FORCE MS 818 AFM/SPM instrument. Cyclic voltammograms were measured in CH_2Cl_2 containing 0.1 M TBAF and 1×10^{-3} M analyte on a CH Instrument equipment (Model 600A). A three-electrode configuration was employed with a Pt disk as the working electrode, a silver wire as the auxiliary electrode, and a $Ag/AgNO_3$ reference electrode. The redox potentials were referenced to the ferrocene/ferrocenium redox couple. Crystallographic data were collected on a Bruker SMART Apex CCD diffractometer with Mo Kα radiation (λ = 0.71073 Å). CCDC-1031429, CCDC-1031430, and CCDC-1031431 contain the supplementary crystallographic data for this paper. These data can be obtained free of charge from The Cambridge Crystallographic Data Centre via www.ccdc.cam.ac.uk/data_request/cif.

Procedure for the Synthesis of ICDP: A solution of DMIC (2.00 mmol), sodium *t*-butoxide (6.00 mmol), $Pd_2(dba)_3$ (0.060 mmol), tri-*t*-butylphosphine (0.10 mmol), and PhI (6.00 mmol) in *o*-xylene (6.0 mL) was heated under a nitrogen atmosphere at 150 °C for 48 h. After cooling to room temperature, the resulting mixture was filtered through a Celite and silica gel pad and the pad was further washed with dichloromethane. The combined filtrate was concentrated under reduced pressure and the residue was purified on silica gel column by using hexane/ethyl acetate as eluent to afford the desired product ICDP. The product was further purified by sublimation to give the pure ICDP in 64% yield. ^{1}H NMR (400 MHz, $CDCl_3$, δ): 7.53 (d, J = 4.4 Hz, 1 H), 7.64–7.30 (m, 13 H), 7.12 (t, J = 6.8 Hz, 1 H), 6.98 (d, J = 8.4 Hz, 1 H), 6.69 (t, J = 6.8 Hz, 1 H), 5.89 (d, J = 8.4 Hz, 1 H), 2.97 (s, 3 H), 2.10 (s, 3 H); ^{13}C NMR (100 MHz, $CDCl_3$, δ): 142.7 (C), 142.2 (C), 141.1 (C), 140.8 (C), 135.2 (C), 131.0 (C), 129.8 (2 CH), 129.3 (2 CH), 129.1 (4 CH), 128.1 (CH), 127.9 (CH), 124.9 (C), 123.8 (CH), 123.6 (CH), 123.0 (C), 121.8 (CH), 121.5 (C), 120.1 (CH), 119.3 (CH), 117.0 (C), 112.9 (2 C), 110.0 (CH), 109.8 (CH), 107.2 (C), 17.3 (CH_3), 15.7 (CH_3); HRMS (EI) m/z: $[M]^+$ calcd for $C_{32}H_{24}N_2$, 436.1939; found, 436.1935.

Preparation of 6,7-dimethyl-12-(pyridin-4-yl)-5,12-dihydroindolo[3,2-a] carbazole (4ICPy): The preparation procedure for 4ICPy is similar to that for ICDP except that DMIC (2.0 mmol) and 4-bromopyridine (2.2 mmol) were used as the reactants. The desired product was obtained as a pale yellow solid (yield 29%). ^{1}H NMR (400 MHz, $CDCl_3$, δ): 8.82 (br, 2 H), 8.32 (m, 2 H), 7.52–7.48 (m, 4 H), 7.38–7.35 (m, 2 H), 7.26 (t, J = 8.0 Hz, 1 H), 6.83 (t, J = 7.2 Hz, 1 H), 6.04 (d, J = 8.0 Hz, 1 H), 3.02 (s, 3 H), 2.66 (s, 3 H); ^{13}C NMR (100 MHz, $CDCl_3$, δ): 151.5 (2 CH), 147.9 (C), 140.6 (C), 139.8 (C), 138.7 (C), 134.0 (C), 129.6 (C), 126.2 (C), 124.2 (CH), 123.8 (CH), 123.0 (2 CH), 122.8 (CH), 121.9 (CH), 121.2 (CH), 119.1 (CH), 117.2 (C), 112.0 (2 C), 110.2 (CH), 109.6 (CH), 105.5 (C), 17.0 (CH_3), 13.3 (CH_3); HRMS (EI) m/z: $[M]^+$ calcd for $C_{25}H_{19}N_3$, 361.1579; found, 361.1586.

Preparation of 4ICPPy: 4ICPPy was synthesized via a procedure similar to the above one by using 4ICPy (2.0 mmol) and iodobenzene (2.2 mmol) as the reactants. The desired product was further sublimed to give pure 4ICPPy in 60% yield. ^{1}H NMR (400 MHz, $CDCl_3$, δ): 8.79 (d, J = 6.8 Hz, 4 H), 8.34 (m, 1 H), 7.67 (d, J = 4.8 Hz, 1 H), 7.60–7.19 (m, 9 H), 7.05 (d, J = 8.4 Hz, 1 H), 6.86 (t, J = 8.0 Hz, 1 H), 6.20 (d, J = 8.0 Hz, 1 H), 2.95 (s, 3 H), 2.14 (s, 3 H); ^{13}C NMR (100 MHz, $CDCl_3$, δ):151.4 (2 CH), 148.2 (C), 142.8 (C), 141.1 (C), 141.0 (C), 140.8 (C), 133.9 (C), 131.0 (C), 129.4 (2 CH), 129.1 (2 CH), 128.1 (CH), 126.1 (C), 124.3 (CH), 124.1 (CH), 122.7 (CH), 122.5 (2 CH), 122.1 (CH), 121.3 (CH), 120.9 (C), 119.5 (CH), 118.1 (C), 114.2 (2 C), 110.0 (CH), 109.8 (CH), 107.4 (C), 17.2 (CH_3), 15.6 (CH_3); HRMS (EI) m/z: $[M]^+$ calcd for $C_{31}H_{23}N_3$, 437.1892; found, 437.1895.

Preparation of 4ICDPy: 4ICDPy was synthesized *via* a similar procedure for the preparation of ICDP (see above) but using DMIC and 4-bromopyridine as the reactants. The desired product was further sublimed to give the pure 4ICDPy in 43% yield. ^{1}H NMR (400 MHz, $CDCl_3$, δ): 8.82 (td, J = 4.8 Hz, 1.6 Hz, 4 H), 8.34 (dd, J = 6.0 Hz, 2.0 Hz, 1 H), 7.57 (dd, J = 4.8 Hz, 2.0 Hz, 1 H), 7.48 (dd, J = 6.0 Hz, 1.6 Hz, 2 H), 7.43–7.18 (m, 6 H), 6.85 (dt, J = 6.0 Hz, 2.0 Hz, 1 H), 6.15 (d, J = 8.4 Hz, 1 H), 2.95 (s, 3 H), 2.14 (s, 3 H); ^{13}C NMR (100 MHz, $CDCl_3$, δ): 151.5 (2 CH), 151.2 (2 CH), 148.8 (C), 148.0 (C), 141.7 (C), 141.3 (C), 140.6 (C), 133.9 (C), 125.8 (C), 124.8 (CH), 124.5 (CH), 123.2 (2 CH), 123.0 (CH), 122.5 (2 CH), 122.3 (CH), 122.0 (C), 121.5 (CH), 120.5 (CH), 119.2 (C), 114.2 (2 C), 109.9 (CH), 109.7 (CH), 108.5 (C), 17.2 (CH_3), 16.8 (CH_3); HRMS (EI) m/z: $[M]^+$ calcd for $C_{30}H_{22}N_4$, 438.1844; found, 438.1839.

Theoretical Calculation: Quantum-chemical simulation of molecular geometries and electronic states were conducted based on DFT formalism, implemented in Gaussian 09 program package. The B3LYP method (the hybrid three parameter Becke exchange functional combined with the Lee–Yang–Parr correlation functional) with the 6–31G* basic set were employed for all atoms. The singlet excited-state properties were performed using TD-DFT approach with B3LYP functional, and were analyzed *via* natural transition orbital.

OLED Fabrication and Measurements: Prior to the fabrication of EL devices, ITO electrode substrate with a sheet resistance of 15 Ω sq^{-1} was cleaned utilizing neutral detergent, distilled water, and acetone. Then, the substrate was treated with UV-ozone for 10 min. The organic materials were thermally evaporated onto the ITO substrate with a rate of 1–2 Å s^{-1} in the vacuum of 10^{-6} Torr. The cathode composed of LiF/Al was completed *via* thermal deposition of LiF at a rate of 0.1 Å s^{-1} and then capped with Al metal deposited at a rate of 5 Å s^{-1}. The effective emitting area of EL devices was 9.00 mm^2. The voltage–current–luminance characteristics measurements were made simultaneously using a Keithley 2400 source meter and a Newport 1835-C optical meter equipped with a calibrated silicon photodiode (Newport 818-ST).[5] Electroluminescence spectra were measured on a Konica Minolta CS-2000 spectroradiometer. The hole- and electron-only devices with respective configurations of ITO/MoO_3 (1 nm)/host (100 nm)/MoO_3 (10 nm)/Al and ITO/Ca (5 nm)/host (100 nm)/LiF (1 nm)/Al were fabricated to study carrier mobility of indolocarbazole-based hosts. The hole and electron mobility were evaluated by means of SCLC technique.

Supporting Information

Supporting Information is available from the Wiley Online Library or from the author.

Acknowledgements

The authors thank the Ministry of Science and Technology of the Republic of China (MOST 103–2633-M-007–001) for financial support of this research and the National Center for High-Performance Computing (Account No.: u32chc04) for providing the computing time.

Received: May 20, 2015
Revised: June 27, 2015
Published online: August 6, 2015

[1] a) C. W. Han, Y. H. Tak, B. C. Ahn, *J. Soc. Inf. Disp.* **2011**, *19*, 190; b) S. Mukherjee, P. Thilagar, *Dyes Pigments* **2014**, *110*, 2; c) L. L. Deng, H. W. Zhou, S. F. Chen, H. Y. Shi, B. Liu, L. H. Wang, W. Huang, *J. Appl. Phys.* **2015**, *117*, 083113; d) G. M. Farinola, R. Ragni, *Chem. Soc. Rev.* **2011**, *40*, 3467; e) B. W. D'Andrade, S. R. Forrest, *Adv. Mater.* **2004**, *16*, 1585; f) G. J. Zhou, W. Y. Wong, S. Suo, *J. Photochem. Photobiol., C* **2010**, *11*, 133.

[2] M. A. Baldo, D. F. O'Brien, Y. You, A. Shoustikov, S. Sibley, M. E. Thompson, S. R. Forrest, *Nature* **1998**, *395*, 151.

[3] S. J. Yeh, M. F. Wu, C. T. Chen, Y. H. Song, Y. Chi, M. H. Ho, S. F. Hsu, C. H. Chen, *Adv. Mater.* **2005**, *17*, 285.

[4] a) M. A. Baldo, M. E. Thompson, S. R. Forrest, *Nature* **2000**, *403*, 750; b) T.-Y. Hwu, T.-C. Tsai, W.-Y. Hung, S.-Y. Chang, Y. Chi, M.-H. Chen, C.-I. Wu, K.-T. Wong, L.-C. Chi, *Chem. Commun.* **2008**, 4956; c) J.-J. Lin, W.-S. Liao, H.-J. Huang, F.-I. Wu, C.-H. Cheng, *Adv. Funct. Mater.* **2008**, *18*, 485; d) C. L. Ho, W. Y. Wong, *New J. Chem.*

2013, *37*, 1665; e) H. Sasabe, J. Kido, *J. Mater. Chem. C* **2013**, *1*, 1699; f) G. L. Ingram, Z. H. Lu, *J. Photonics Energy* **2014**, *4*, 18.
[5] H.-H. Chou, C.-H. Cheng, *Adv. Mater.* **2010**, *22*, 2468.
[6] A. Chaskar, H.-F. Chen, K.-T. Wong, *Adv. Mater.* **2011**, *23*, 3876.
[7] a) Y.-Y. Lyu, J. Kwak, W. S. Jeon, Y. Byun, H. S. Lee, D. Kim, C. Lee, K. Char, *Adv. Funct. Mater.* **2009**, *19*, 420; b) Y. Tao, S. Gong, Q. Wang, C. Zhong, C. Yang, J. Qin, D. Ma, *Phys. Chem. Chem. Phys.* **2010**, *12*, 2438.
[8] a) S. H. Cheng, W. Y. Hung, M. H. Cheng, H. F. Chen, A. Chaskar, G. H. Lee, S. H. Chou, K. T. Wong, *J. Mater. Chem. C* **2014**, *2*, 8554; b) P. Kautny, D. Lumpi, Y. P. Wang, A. Tissot, J. Bintinger, E. Horkel, B. Stoger, C. Hametner, H. Hagemann, D. G. Ma, J. Frohlich, *J. Mater. Chem. C* **2014**, *2*, 2069; c) X. D. Wang, S. M. Wang, Z. H. Ma, J. Q. Ding, L. X. Wang, X. B. Jing, F. S. Wang, *Adv. Funct. Mater.* **2014**, *24*, 3413; d) L. Ding, S. C. Dong, Z. Q. Jiang, H. Chen, L. S. Liao, *Adv. Funct. Mater.* **2015**, *25*, 645; e) B. Pan, B. Wang, Y. Wang, P. Xu, L. Wang, J. Chen, D. Ma, *J. Mater. Chem. C* **2014**, *2*, 2466.
[9] a) C.-H. Chang, M.-C. Kuo, W.-C. Lin, Y.-T. Chen, K.-T. Wong, S.-H. Chou, E. Mondal, R. C. Kwong, S. Xia, T. Nakagawa, C. Adachi, *J. Mater. Chem.* **2012**, *22*, 3832; b) L. S. Cui, Y. Liu, X. D. Yuan, Q. Li, Z. Q. Jiang, L. S. Liao, *J. Mater. Chem. C* **2013**, *1*, 8177; c) D. D. Zhang, L. Duan, Y. L. Li, H. Y. Li, Z. Y. Bin, D. Q. Zhang, J. Qiao, G. F. Dong, L. D. Wang, Y. Qiu, *Adv. Funct. Mater.* **2014**, *24*, 3551.
[10] S. Gong, Y. Chen, C. Yang, C. Zhong, J. Qin, D. Ma, *Adv. Mater.* **2010**, *22*, 5370.
[11] a) S.-H. Chou, W.-Y. Hung, C.-M. Chen, Q.-Y. Liu, Y.-H. Liu, K.-T. Wong, *RSC Adv.* **2013**, *3*, 13891; b) E. Mondal, W.-Y. Hung, H.-C. Dai, K.-T. Wong, *Adv. Funct. Mater.* **2013**, *23*, 3096.
[12] a) I. Levesque, P.-O. Bertrand, N. Blouin, M. Leclerc, S. Zecchin, G. Zotti, C. I. Ratcliffe, D. D. Klug, X. Gao, F. Gao, J. S. Tse, *Chem. Mater.* **2007**, *19*, 2128; b) J.-M. Suk, J.-I. Kim, K.-S. Jeong, *Chem. Asian J.* **2011**, *6*, 1992; c) P. Gong, P. Xue, C. Qian, Z. Zhang, R. Lu, *Org. Biomol. Chem.* **2014**, *12*, 6134; d) J. H. Park, H. S. Lee, S. Park, S.-W. Min, Y. Yi, C.-G. Cho, J. Han, T. W. Kim, S. Im, *Adv. Funct. Mater.* **2014**, *24*, 1109.
[13] a) N. X. Hu, S. Xie, Z. Popovic, B. Ong, A. M. Hor, S. N. Wang, *J. Am. Chem. Soc.* **1999**, *121*, 5097; b) N. X. Hu, S. Xie, Z. D. Popovic, B. Ong, A. M. Hor, *Synth. Met.* **2000**, *111*, 421; c) S. Wakim, J. Bouchard, M. Simard, N. Drolet, Y. Tao, M. Leclerc, *Chem. Mater.* **2004**, *16*, 4386; d) H.-P. Zhao, X.-T. Tao, P. Wang, Y. Ren, J.-X. Yang, Y.-X. Yan, C.-X. Yuan, H.-J. Liu, D.-C. Zou, M.-H. Jiang, A. Jiang, *Org. Electron.* **2007**, *8*, 673; e) S. Lengvinaite, J. V. Grazulevicius, S. Grigalevicius, R. Gu, W. Dehaen, V. Jankauskas, B. Zhang, Z. Xie, *Dyes Pigments* **2010**, *85*, 183; f) H.-C. Ting, Y.-M. Chen, H.-W. You, W.-Y. Hung, S.-H. Lin, A. Chaskar, S.-H. Chou, Y. Chi, R.-H. Liu, K.-T. Wong, *J. Mater. Chem.* **2012**, *22*, 8399; g) H.-C. Ting, C.-H. Tsai, J.-H. Chen, L.-Y. Lin, S.-H. Chou, K.-T. Wong, T.-W. Huang, C.-C. Wu, *Org. Lett.* **2012**, *14*, 6338; h) G. Zhao, H. Dong, H. Zhao, L. Jiang, X. Zhang, J. Tan, Q. Meng, W. Hu, *J. Mater. Chem.* **2012**, *22*, 4409; i) S. Chen, J. Wei, K. Wang, C. Wang, D. Chen, Y. Liu, Y. Wang, *J. Mater. Chem. C* **2013**, *1*, 6594; j) J.-Y. Su, C.-Y. Lo, C.-H. Tsai, C.-H. Chen, S.-H. Chou, S.-H. Liu, P.-T. Chou, K.-T. Wong, *Org. Lett.* **2014**, *16*, 3176.
[14] a) M. Romain, D. Tondelier, J.-C. Vanel, B. Geffroy, O. Jeannin, J. Rault-Berthelot, R. Metivier, C. Poriel, *Angew. Chem. Int. Ed.* **2013**, *52*, 14147; b) M. Romain, S. Thiery, A. Shirinskaya, C. Declairieux, D. Tondelier, B. Geffroy, O. Jeannin, J. Rault-Berthelot, R. Metivier, C. Poriel, *Angew. Chem. Int. Ed.* **2015**, *54*, 1176.
[15] a) H. Sasabe, D. Tanaka, D. Yokoyama, T. Chiba, Y.-J. Pu, K.-i. Nakayama, M. Yokoyama, J. Kido, *Adv. Funct. Mater.* **2011**, *21*, 336; b) C. Meier, U. Ziener, K. Landfester, P. Weihrich, *J. Phys. Chem. B* **2005**, *109*, 21015.
[16] V. Nair, V. Nandialath, K. G. Abhilash, E. Suresh, *Org. Biomol. Chem.* **2008**, *6*, 1738.
[17] a) V. A. Galievsky, S. I. Druzhinin, A. Demeter, P. Mayer, S. A. Kovalenko, T. A. Senyushkina, K. A. Zachariasse, *J. Phys. Chem. A* **2010**, *114*, 12622; b) A. Baschieri, L. Sambri, I. Gualandi, D. Tonelli, F. Monti, A. Degli Esposti, N. Armaroli, *RSC Adv.* **2013**, *3*, 6507; c) S.-H. Cheng, W.-Y. Hung, M.-H. Cheng, H.-F. Chen, A. Chaskar, G.-H. Lee, S.-H. Chou, K.-T. Wong, *J. Mater. Chem. C* **2014**, *2*, 8554.
[18] a) S. Zhang, L. Yao, Q. Peng, W. Li, Y. Pan, R. Xiao, Y. Gao, C. Gu, Z. Wang, P. Lu, F. Li, S. Su, B. Yang, Y. Ma, *Adv. Funct. Mater.* **2015**, *25*, 1755; b) W. Li, Y. Pan, R. Xiao, Q. Peng, S. Zhang, D. Ma, F. Li, F. Shen, Y. Wang, B. Yang, Y. Ma, *Adv. Funct. Mater.* **2014**, *24*, 1609.
[19] a) W. Li, D. Liu, F. Shen, D. Ma, Z. Wang, T. Feng, Y. Xu, B. Yang, Y. Ma, *Adv. Funct. Mater.* **2012**, *22*, 2797; b) F.-M. Hsu, C.-H. Chien, C.-F. Shu, C.-H. Lai, C.-C. Hsieh, K.-W. Wang, P.-T. Chou, *Adv. Funct. Mater.* **2009**, *19*, 2834; c) J.-P. Malval, F. Morlet-Savary, H. Chaumeil, L. Balan, D.-L. Versace, M. Jin, A. Defoin, *J. Phys. Chem. C* **2009**, *113*, 20812; d) C. Garcia, R. Oyola, L. Pinero, D. Hernandez, R. Arce, *J. Phys. Chem. B* **2008**, *112*, 168.
[20] Murgatro. Pn, *J. Phys. D: Appl. Phys.* **1970**, *3*, 151.
[21] T. Ogawa, D. C. Cho, K. Kaneko, T. Mori, T. Mizutani, *Thin Solid Films* **2003**, *438*, 171.
[22] X. Wang, Y. L. Chang, J. S. Lu, T. Zhang, Z. H. Lu, S. N. Wang, *Adv. Funct. Mater.* **2014**, *24*, 1911.
[23] a) H. Murata, C. D. Merritt, Z. H. Kafafi, *IEEE J. Sel. Top. Quantum Electron.* **1998**, *4*, 119; b) T. L. Chiu, P. Y. Lee, *Int. J. Mol. Sci.* **2012**, *13*, 7575.
[24] Y. J. Cho, K. S. Yook, J. Y. Lee, *Adv. Mater.* **2014**, *26*, 4050.
[25] a) C. L. Ho, L. C. Chi, W. Y. Hung, W. J. Chen, Y. C. Lin, H. Wu, E. Mondal, G. J. Zhou, K. T. Wong, W. Y. Wong, *J. Mater. Chem.* **2012**, *22*, 215; b) E. Mondal, W. Y. Hung, H. C. Dai, K. T. Wong, *Adv. Funct. Mater.* **2013**, *23*, 3096; c) P. Kautny, D. Lumpi, Y. Wang, A. Tissot, J. Bintinger, E. Horkel, B. Stoeger, C. Hametner, H. Hagemann, D. Ma, J. Froehlich, *J. Mater. Chem. C* **2014**, *2*, 2069.
[26] Q. Wang, D. G. Ma, *Chem. Soc. Rev.* **2010**, *39*, 2387.
[27] Z. B. Wang, M. G. Helander, J. Qiu, D. P. Puzzo, M. T. Greiner, Z. W. Liu, Z. H. Lu, *Appl. Phys. Lett.* **2011**, *98*, 073310.
[28] a) Y. Yin, X. Piao, Y. Li, Y. Wang, J. Liu, K. Xu, W. Xie, *Appl. Phys. Lett.* **2012**, *101*, 063306; b) Y. X. Zhang, L. Zhang, L. S. Cui, C. H. Gao, H. Chen, Q. Li, Z. Q. Jiang, L. S. Liao, *Org. Lett.* **2014**, *16*, 3748; c) Y. Qian, Y. Ni, S. Yue, W. Li, S. Chen, Z. Zhang, L. Xie, M. Sun, Y. Zhao, W. Huang, *RSC Adv.* **2015**, *5*, 29828.